532. 543 : 621-288

# An Investigation of Air-leakage between Contact Surfaces*

By Tsuneji KAZAMAKI**

In this paper, the mechanism of air-leakage between contact surfaces was studied. The mechanical properties of modeled surface irregularities in a shape of truncated cones were assumed to be ideally plastic or elastic.

The results obtained can be summarized that the theoretical values of equivalent gap between contact surfaces agree with those obtained from experiments within an error of about 7 %.

## 1. Introduction

Fluid leakage between contact surfaces is a phenomenon resulting from the interaction of the microgeometric forms of surface irregularities of the contact surfaces and their elastoplastic deformations and the fluid pressure distribution between them.

In the past some studies on the contact surfaces including surface roughness and the deformation of contact surfaces in relation to leakage were published [1] [2].

In this paper, we assumed the microscopic truncated cones for the surface irregularities and considered two cases in which the mechanical property of the microscopic irregularities was assumed to be ideally elastic or plastic.

Theoretical expressions for the equivalent gap between contact surfaces with respect to fluid leakage were derived and verified with the experimental results.

## 2. Nomenclature

$H$ : height of various surface irregularities
$H_{\max}$ : maximum height of various surface irregularities
$h_c$ : central height of surface irregularities
$H_e$ : equivalent gap between contact surfaces (without applied load)
$H_{ep}$ : ditto (with applied load)
$\Delta H$ : displacement of surface irregularities due to applied load
$Z_0=H_{\max}-\Delta H$
$s_0$ : upper area of various truncated cones
$s_a$ : bottom area of various truncated cones
$s=s_a/s_0$
$s_z$ : sectional area at different positions of various truncated cones
$S_a$ : total bottom area for various truncated cones
$S_n$ : nominal area of contact surface
$2r$ : conical angle of various truncated cones
$\xi_{e1}$, $\xi_{p1}$ : displacement due to elastic and plastic deformations for various truncated cones
$P_m$ : applied load on any truncated cone
$P_c$ : total applied load on nominal area
$M$ : total number of various truncated cones
$N$ : number of various truncated cones in contact due to applied load
$V$ : total volume of various truncated cones
$f_{(H)}$ : distribution function for surface roughness irregularities
$\alpha$ : parameter of $f_{(H)}$
$\beta=Z_0/\alpha$
$\varphi_{(\beta)}$, $\Phi_{(\beta)}$, $\Psi_{(\beta)}$ : functions for $\beta$
$E$ : Young's modulus of specimens
$\sigma_s$ : yield point of specimens
$k$ : function of conical angle of various truncated cones
$q$ : air flow rate per unit width at contact surface
$Q$ : total flow rate of air-leakage
$Q_i$ : total flow rate of air-leakage converted into a state of outlet air pressure
$G$ : total weight of air-leakage
$p_a$ : inlet air pressure ; absolute pressure
$p_a^*$ : ditto ; gauge pressure
$p_i$ : outlet air pressure ; absolute pressure
$\Delta p=p_a-p_i$
$r$ : radius of any point on contact surface
$r_o$ : outer radius of contact surfaces
$r_i$ : inner radius of contact surfaces
$r_{oi}=r_o/r_i$
$\mu$ : absolute viscosity of air
$v$ : specific volume of air at any position on contact surfaces

* Received 20th October, 1967.
** Assistant Professor, Faculty of Engineering, Toyama University, Takaoka.

$v_i$: specific volume of outlet air

## 3. Equivalent gap between contact surfaces; $H_{ep}$

Assuming that the profile of surface irregularities is given as shown in Fig. 1, the equivalent gap between contact surfaces may be defined in the case of no load being applied as follows.

$$H_e=H_{\max}-h_c \quad \cdots\cdots(1)$$

Hence, the gap when a body having this surface roughness is pressed against a rigid body having an ideal smooth surface is given as follows:

$$H_{ep}=H_e-\Delta H=Z_0-h_c \quad \cdots\cdots(2)$$

Where the values of $H_{ep}$ may be related to the geometrical forms of the surface irregularities, their elastoplastic properties and the applied load. In deriving the theoretical expressions we assumed the mechanical property of the surface irregularities to be ideally elastic or plastic.

Furthermore, we make assumptions as follows:

(1) The irregularities have a form of geometrically similar truncated cone.

(2) The irregularities have their respective cone bases in the supposed base plane.

### 3·1 The case in which the truncated cones are assumed to be ideally elastic

Let the truncated cone be as shown in Fig. 2, then $s_z$ is given as follows:

$$s_z=\pi\tan^2\gamma\left(\frac{H}{\sqrt{s}-1}+z\right)^2$$

It follows that the displacement $d\xi_{el}$ of a small portion $dz$ of a truncated cone subjected to load $P_m$ becomes

$$d\xi_{el}=\frac{P_m}{E}\frac{dz}{\pi\tan^2\gamma\left(\frac{H}{\sqrt{s}-1}+z\right)^2}$$

Then

$$\xi_{el}=\int_0^H\frac{P_m}{E}\frac{dz}{\pi\tan^2\gamma\left(\frac{H}{\sqrt{s}-1}+z\right)^2}=\frac{P_m}{\pi E\tan^2\gamma}\frac{(\sqrt{s}-1)^2}{\sqrt{s}H} \quad \cdots\cdots(3)$$

Since, in this case, the surface irregularities are pressed against a rigid surface, the irregularities subjected to actual contact must be at the height $Z_0$ from the base plane.

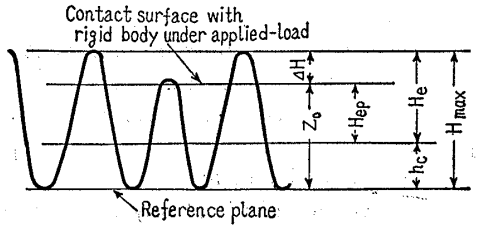


Fig. 1 Profile of surface irregularities

Therefore

$$H-\xi_{el,pl}\equiv Z_0 \quad \cdots\cdots(4)$$

Thus, Eq. (3) becomes

$$P_m=\pi E\tan^2\gamma\frac{\sqrt{s}H}{(\sqrt{s}-1)^2}(H-Z_0) \quad \cdots\cdots(5)$$

Here, Krasavin[3] obtained the following experimental expression for the distribution function of surface roughness $H$:

$$f_{(H)}=CH^2\exp(-H^2/\alpha^2) \quad \cdots\cdots(6)$$

If we apply this relation to Eq. (5), the total applied load is obtained as follows:

$$P_c=N\int_{Z_0}^{\infty}P_m f_{(H)}dH \quad \cdots\cdots(7)$$

Substituting Eq. (5) in Eq. (7) gives

$$\begin{aligned}P_c&=\frac{\pi E\tan^2\gamma\sqrt{s}}{(\sqrt{s}-1)^2}NC\int_{Z_0}^{\infty}(H-Z_0)H^3e^{-H^2/\alpha^2}dH\\&=\frac{\pi E\tan^2\gamma\sqrt{s}}{(\sqrt{s}-1)^2}NC\left[\int_{Z_0}^{\infty}H^4e^{-H^2/\alpha^2}dH-Z_0\int_{Z_0}^{\infty}H^3e^{-H^2/\alpha^2}dH\right]\\&=\pi E\tan^2\gamma\frac{\sqrt{s}}{(\sqrt{s}-1)^2}NC\left[\frac{3}{8}\sqrt{\pi}\alpha^5+\frac{\alpha^5}{2}e^{-Z_0^2/\alpha^2}\frac{Z_0^3}{\alpha^3}+\frac{\alpha^5}{2}\frac{3}{2}e^{-Z_0^2/\alpha^2}\frac{Z_0}{\alpha}-\frac{3}{4}\alpha^5\int_0^{Z_0/\alpha}e^{-\lambda^2}d\lambda-Z_0\left\{\frac{\alpha^4}{2}e^{-Z_0^2/\alpha^2}\left(\frac{Z_0^2}{\alpha^2}+1\right)\right\}\right]\\&=\pi E\tan^2\gamma\frac{\sqrt{s}}{(\sqrt{s}-1)^2}\frac{3}{8}\sqrt{\pi}NC\alpha^5\times\left[1+\frac{2}{3\sqrt{\pi}}\beta e^{-\beta^2}-\frac{2}{\sqrt{\pi}}\int_0^{\beta}e^{-\lambda^2}d\lambda\right]\end{aligned} \quad \cdots(8)$$

Here, the distribution of surface roughness signifies a probability distribution ranging from zero to infinity, and the distribution function $f_{(H)}$ must satisfy the following relation:

$$\int_0^{\infty}f_{(H)}dH\equiv 1$$

If we apply this relation to Eq. (6), the coefficient $C$ is determined as follows:

$$\left.\begin{aligned}&C\int_0^{\infty}H^2e^{-H^2/\alpha^2}dH=C\frac{\sqrt{\pi}}{4}\alpha^3=1\\&C=4/(\sqrt{\pi}\alpha^3)\end{aligned}\right\} \quad \cdots\cdots(9)$$

Also, from Fig. 2, $s_a$ is given as follows:

$$s_a=\pi\tan^2\gamma H^2 s/(\sqrt{s}-1)^2$$

Then

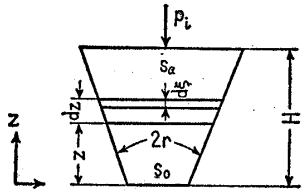


Fig. 2 A truncated model of surface irregular part

$$S_a=\int_0^\infty s_a f_{(H)}\,dH$$

$$=\pi\tan^2\gamma(3/2)\alpha^2 s/(\sqrt{s}-1)^2 \quad \cdots\cdots(10)$$

Here, from the assumption (2) the total number $M$ of the irregularities becomes

$$M=S_n/S_a=\frac{S_n}{\pi\tan^2\gamma}\frac{2}{3}\frac{1}{\alpha^2}\frac{(\sqrt{s}-1)^2}{s} \quad \cdots\cdots(11)$$

Then, the number $N$ of the irregularities may be calculated as

$$N=\int_{Z_0}^\infty M f_{(H)}\,dH$$

$$=M\left[1+\frac{2}{\sqrt{\pi}}\beta e^{-\beta^2}-\frac{2}{\sqrt{\pi}}\int_0^\beta e^{-\lambda^2}d\lambda\right]$$

Here, we replace the terms of the brackets by dimensionless quantities $\varphi_{(\beta)}$ as follows:

$$N=M\varphi_{(\beta)}$$

$$\varphi_{(\beta)}=1+\frac{2}{\sqrt{\pi}}\beta e^{-\beta^2}-\frac{2}{\sqrt{\pi}}\int_0^\beta e^{-\lambda^2}d\lambda$$

For varying values of $\beta$ we have calculated $\varphi_{(\beta)}$, and the values of this function for $\beta=0.1\sim2.0$ are listed in Table 1.

Therefore, the number $N$ will be expressed as follows:

$$N\fallingdotseq M(1.117e^{-0.72\beta^2})$$

$$=\frac{0.7446}{\pi}\frac{S_n}{\tan^2\gamma}\frac{(\sqrt{s}-1)^2}{s}\frac{e^{-0.72\beta^2}}{\alpha^2} \quad \cdots\cdots(12)$$

Introducing Eqs. (9) and (12) into Eq. (8), the total applied load will be described as follows:

$$P_c=1.117\frac{S_n}{\sqrt{s}}Ee^{-0.72\beta^2}\left[1+\frac{2}{3\sqrt{\pi}}\beta e^{-\beta^2}-\frac{2}{\sqrt{\pi}}\int_0^\beta e^{-\lambda^2}d\lambda\right]$$

In the same manner as above we put

$$\Phi_{(\beta)}=1+\frac{2}{3\sqrt{\pi}}\beta e^{-\beta^2}-\frac{2}{\sqrt{\pi}}\int_0^\beta e^{-\lambda^2}d\lambda$$

For varying values of $\beta$ we have calculated $\Phi_{(\beta)}$, and the values of this function for $\beta=0.1\sim2.0$ are listed in Table 2.

Therefore

$$P_c\fallingdotseq1.117\frac{S_n}{\sqrt{s}}Ee^{-0.72\beta^2}(0.771e^{-0.958\beta^2})$$

$$=0.861\frac{S_n}{\sqrt{s}}Ee^{-1.678\beta^2} \quad \cdots\cdots(13)$$

Then the height from the base plane will be described by

$$Z_0=\alpha\sqrt{\frac{1}{1.678}\ln\left\{\frac{0.861}{\sqrt{s}}\frac{S_n}{P_c}E\right\}} \quad \cdots\cdots(14)$$

The unknown term $\alpha$ in Eq. (14) may be obtained from the following expression for the total volume $V$ of the truncated cones.

$$V=M\int_0^\infty\left[\frac{\pi}{3}\left\{\left(\frac{H}{\sqrt{s}-1}+H\right)^3\tan^2\gamma-\left(\frac{H}{\sqrt{s}-1}\right)^3\tan^2\gamma\right\}\right]f_{(H)}\,dH$$

$$=\frac{8}{9\sqrt{\pi}}\frac{(s+\sqrt{s}+1)}{s}S_n\alpha \quad \cdots\cdots(15)$$

We now introduce the idea of "mean plane" for the central height $h_c$, which is the plane such that the volume of the truncated cones above it is equal to the volume of empty space below it:

$$V=S_n h_c$$

Then

$$\alpha=\frac{9\sqrt{\pi}}{8}\frac{s}{(s+\sqrt{s}+1)}h_c=\frac{9\sqrt{\pi}}{8}h_c\zeta \quad \cdots\cdots(16)$$

where $\zeta=1/\{1+(1/\sqrt{s})+(1/s)\}$ $\cdots\cdots(17)$

Therefore, the equivalent gap $H_{ep}$ is given by the following expression.

$$H_{ep}=Z_0-h_c=\left[1.539\zeta\sqrt{\ln\left\{\frac{0.861}{\sqrt{s}}\frac{S_n}{P_c}E\right\}}-1\right]h_c \quad \cdots\cdots(18)$$

The characteristic curves represented by Eq. (18) are shown in Fig. 3.

Table 1

| $\beta$ | $\varphi_{(\beta)}$ | $1.117e^{-0.72\beta2}$ |
|---|---|---|
| 0.1 | 0.9992 | 1.1089 |
| 0.2 | 0.9941 | 1.0850 |
| 0.3 | 0.9807 | 1.0468 |
| 0.4 | 0.9562 | 0.9954 |
| 0.5 | 0.9189 | 0.9330 |
| 0.6 | 0.8685 | 0.8619 |
| 0.7 | 0.8060 | 0.7849 |
| 0.8 | 0.7338 | 0.7046 |
| 0.9 | 0.6549 | 0.6234 |
| 1.0 | 0.5724 | 0.5437 |
| 1.1 | 0.4899 | 0.4674 |
| 1.2 | 0.4105 | 0.3960 |
| 1.3 | 0.3367 | 0.3308 |
| 1.4 | 0.2703 | 0.2723 |
| 1.5 | 0.2123 | 0.2208 |
| 1.6 | 0.1631 | 0.1764 |
| 1.7 | 0.1226 | 0.1385 |
| 1.8 | 0.0902 | 0.1083 |
| 1.9 | 0.0651 | 0.0830 |
| 2.0 | 0.0460 | 0.0626 |

$0.4\leqq\beta\leqq1.5$ error$\leqq5.5\%$

Table 2

| $\beta$ | $\Phi_{(\beta)}$ | $0.771e^{-0.958\beta2}$ |
|---|---|---|
| 0.1 | 0.9247 | 0.7636 |
| 0.2 | 0.8496 | 0.7420 |
| 0.3 | 0.7745 | 0.7073 |
| 0.4 | 0.6998 | 0.6614 |
| 0.5 | 0.6259 | 0.6067 |
| 0.6 | 0.5536 | 0.5460 |
| 0.7 | 0.4835 | 0.4821 |
| 0.8 | 0.4165 | 0.4176 |
| 0.9 | 0.3537 | 0.3548 |
| 1.0 | 0.2956 | 0.2957 |
| 1.1 | 0.2431 | 0.2418 |
| 1.2 | 0.1966 | 0.1940 |
| 1.3 | 0.1562 | 0.1527 |
| 1.4 | 0.1219 | 0.1178 |
| 1.5 | 0.0933 | 0.0893 |
| 1.6 | 0.0701 | 0.0663 |
| 1.7 | 0.0517 | 0.0483 |
| 1.8 | 0.0373 | 0.0345 |
| 1.9 | 0.0265 | 0.0242 |
| 2.0 | 0.0184 | 0.0167 |

$0.4\leqq\beta\leqq1.6$ error$\leqq6\%$

### 3·2 The case in which the truncated cones are assumed to be ideally plastic

The amount of plastic deformation of a truncated cone caused by the applied load is given by

Marochkin[4] as

$$\xi_{pl}=\sqrt{\frac{P_m}{\pi k\sigma_s}}\frac{1}{\tan\gamma} \quad \cdots\cdots(19)$$

where $k$ is a function of the angle $\gamma$.

Introducing Eq. (19) into Eq. (4), $P_m$ is given as follows:

$$P_m=\pi k\sigma_s\tan^2\gamma(H-Z_0)^2 \quad \cdots\cdots(20)$$

By a similar procedure to the above section, the total applied load is obtained as follows:

$$P_c=N\int_{Z_0}^{\infty}P_m f_{(H)}\,dH$$
$$=1.117\frac{(\sqrt{s}-1)^2}{s}S_n k\sigma_s e^{-0.72\beta^2}\left[1+\frac{2}{3}\beta^2-\frac{2}{3\sqrt{\pi}}\beta e^{-\beta^2}-\left(1+\frac{2}{3}\beta^2\right)\frac{2}{\sqrt{\pi}}\int_0^{\beta}e^{-\lambda^2}d\lambda\right]$$

Here, we replace the terms of the brackets by dimensionless quantities $\Psi_{(\beta)}$ as follows:

$$\Psi_{(\beta)}=1+\frac{2}{3}\beta^2-\frac{2}{3\sqrt{\pi}}\beta e^{-\beta^2}-\left(1+\frac{2}{3}\beta^2\right)\frac{2}{\sqrt{\pi}}\int_0^{\beta}e^{-\lambda^2}d\lambda$$

Table 3

| $\beta$ | $\Psi_{(\beta)}$ | $0.516e^{-1.365\beta^2}$ |
|---|---|---|
| 0.1 | 0.8562 | 0.5090 |
| 0.2 | 0.7257 | 0.4886 |
| 0.3 | 0.6085 | 0.4563 |
| 0.4 | 0.5044 | 0.4147 |
| 0.5 | 0.4130 | 0.3668 |
| 0.6 | 0.3338 | 0.3156 |
| 0.7 | 0.2661 | 0.2643 |
| 0.8 | 0.2093 | 0.2154 |
| 0.9 | 0.1621 | 0.1707 |
| 1.0 | 0.1238 | 0.1317 |
| 1.1 | 0.0930 | 0.0989 |
| 1.2 | 0.0688 | 0.0722 |
| 1.3 | 0.0501 | 0.0513 |
| 1.4 | 0.0358 | 0.0355 |
| 1.5 | 0.0253 | 0.0240 |
| 1.6 | 0.0175 | 0.0156 |
| 1.7 | 0.0120 | 0.0098 |
| 1.8 | 0.0080 | 0.0062 |
| 1.9 | 0.0052 | 0.0037 |
| 2.0 | 0.0034 | 0.0022 |

$0.6\leqq\beta\leqq1.6$ error$\leqq6.5\,\%$

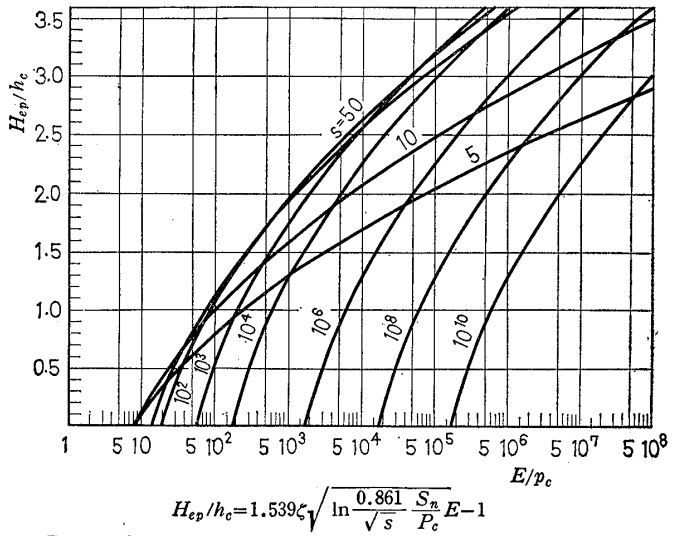


Fig. 3 Characteristic curves; assumed that the truncated cones are ideally elastic

For varying values of $\beta$ we have calculated $\Psi_{(\beta)}$, and the values of this function for $\beta=0.1\sim2.0$ are listed in Table 3.

Therefore

$$P_c\fallingdotseq1.117\frac{(\sqrt{s}-1)^2}{s}S_n k\sigma_s e^{-0.72\beta^2}(0.516e^{-1.365\beta^2})$$
$$=0.576\frac{(\sqrt{s}-1)^2}{s}S_n k\sigma_s e^{-2.085\beta^2} \quad \cdots\cdots(21)$$

Then the height from the base plane will be described by

$$Z_0=\left[1.38\zeta\sqrt{\ln\left\{0.576\frac{(\sqrt{s}-1)^2}{s}\frac{S_n}{P_c}k\sigma_s\right\}}\right]h_c \quad \cdots\cdots(22)$$

Therefore, the equivalent gap $H_{ep}$ is given by the following expression.

$$H_{ep}=\left[1.38\zeta\sqrt{\ln\left\{0.576\frac{(\sqrt{s}-1)^2}{s}\frac{S_n}{P_c}k\sigma_s\right\}}-1\right]h_c \quad \cdots\cdots(23)$$

The characteristic curves represented by Eq. (23) are shown in Fig. 4.

## 4. Fluid leakage between contact surfaces under the applied load

Assuming that the fluid flow is a laminar incompressible flow, the flow rate per unit width of leakage between contact surfaces due to the inlet fluid pressure when a thick cylinder as shown in Fig. 5 is pressed against a rigid body having an ideal smooth surface, i.e., surface roughness $H\cong0$,

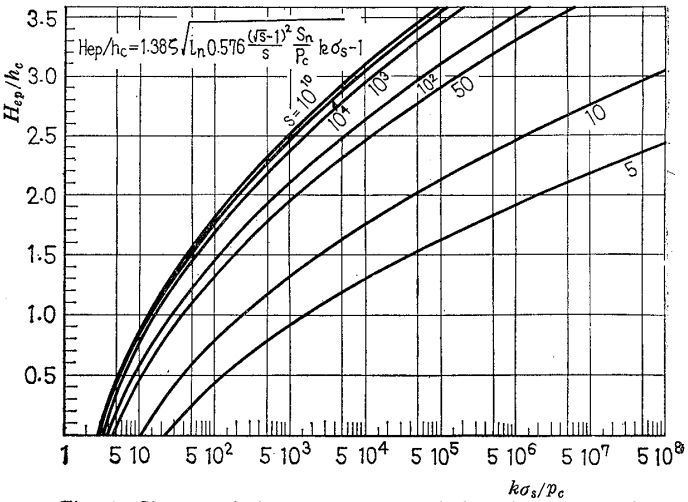


Fig. 4 Characteristic curves; assumed that the truncated cones are ideally plastic

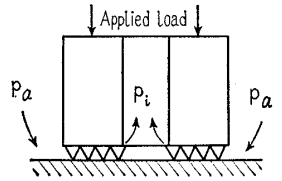


Fig. 5 Schematic diagram for contacts

is given by

$$q=\frac{(H_{ep})^3}{12\mu}\frac{dp}{dr}$$

Assuming that the leakage flow is isothermal, then the expressions are given by

$$\left.\begin{aligned} &G=Q/v=Q_i/v_i \\ &pv=p_iv_i=\text{const.} \end{aligned}\right\} \quad \cdots\cdots(24)$$

Therefore

$$\frac{p_i}{p}Q_i=2\pi r\frac{(H_{ep})^3}{12\mu}\frac{dp}{dr}$$

From above expressions, we have

$$Q_i=\frac{\pi(H_{ep})^3}{12\mu \ln r_{oi}}\frac{(p_a^2-p_i^2)}{p_i} \quad \cdots\cdots(25)$$

## 5. Experiments

### 5·1 Experimental procedure and specimens

Figure 6 shows the outline of the experimental apparatus and Fig. 7 the process of measurement. In order to avoid moisture and dust in the air flow we put desiccant in the first filter and used the second and third filters with a progressively finer mesh.

Using a precision pressure gauge to measure the inlet air pressure, we held the variation of air pressure below 0.01 kg/cm² during the measurement. In the measurement of air-leakage the leaked air was led into an air storage tank submerged in water and the air-leakage quantity was calculated from the rate of weight decrease of the air storage tank before and after the measurement.

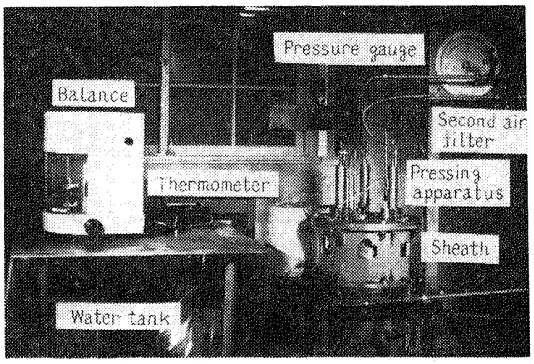


Fig. 6 Experimental apparatus

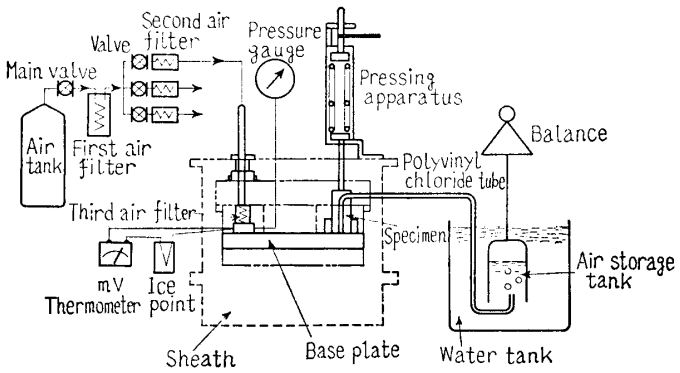


Fig. 7 Process of measurement

Hardened meehanite was used for base plate, and mild steel and carbon steel were used for specimens, the mechanical properties being listed in Table 4 and the form of specimens shown in Fig. 8.

Figure 9 shows the profiles of the surface roughness of the experimental materials, and the numerical values of their surface roughness are listed in Table 5.

Table 4 Mechanical properties of specimens

| Specimens | Yield point $\sigma_s$ kg/mm² | Young's modulus $E\times10^4$ kg/mm² | Hardness $H_B$ |
|---|---|---|---|
| SS 41 | 23.0 | 2.1 | 206 |
| S 45 C | 35.0 | 2.1 | 230 |

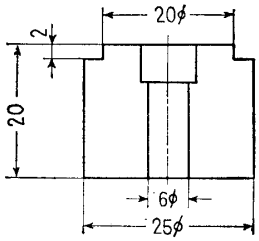


Fig. 8 Form of specimens

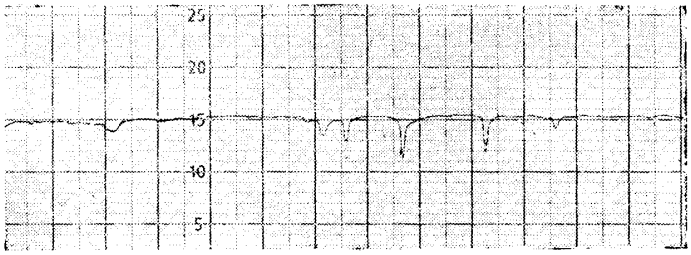

Base plate M-GA Magnification {Ordinate ×10 000 / Abscissa ×500}

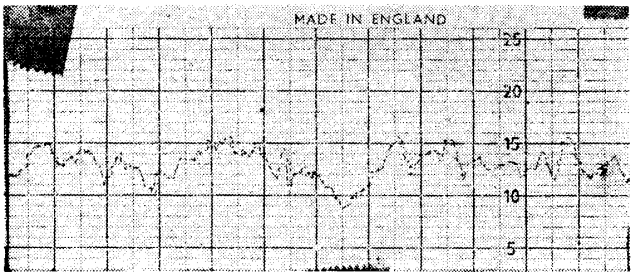


Specimen SS 41 Magnification {Ordinate ×1 000 / Abscissa ×100}

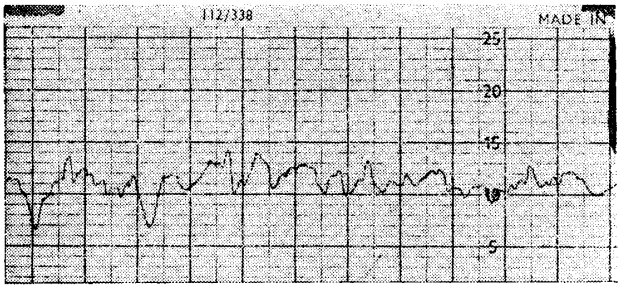

Specimen S 45 C Magnification {Ordinate ×1 000 / Abscissa ×100}

Fig. 9 Profiles of surface roughness

Since in this experiment we are discussing air-leakage between contact surfaces, we need the numerical values having undulating profiles of the whole contact surface. For this purpose, the surface roughness was recorded at three sampled places in radial and tangential directions, respectively, of the contact surface and their mean values were used for theoretical calculation.

Values in the brackets in Table 5 were obtained by using the base plane length prescribed by Japan Industrial Standards.

### 5·2 Experimental results

(1) $\gamma$-values

The conical angle of the truncated cones was determined by using the profiles of the surface roughness obtained in six sampled directions of the specimens. The distribution is shown in Fig. 10;

Table 5 Numerical values of surface roughness

| Materials | | Surface roughness $H_{max}$ | Surface roughness $h_c$ | Processing methods |
|---|---|---|---|---|
| Base plate | M-GA | 0.5 | | Lapping |
| Specimens | SS 41 | 18.0 (13.0) | 5.80 (5.50) | #60 carborundum powder Lapping |
| | S 45 C | 17.0 (12.0) | 5.70 (5.50) | |

(Base plate; hardened Meehanite, Hardness $H_B$=260)

Table 6 Values of $\gamma$ and $k$

| Specimens | $\gamma$ (°) | $k$ |
|---|---|---|
| SS 41 | 76 | 2.385 |
| S 45 C | 80 | 2.46 |

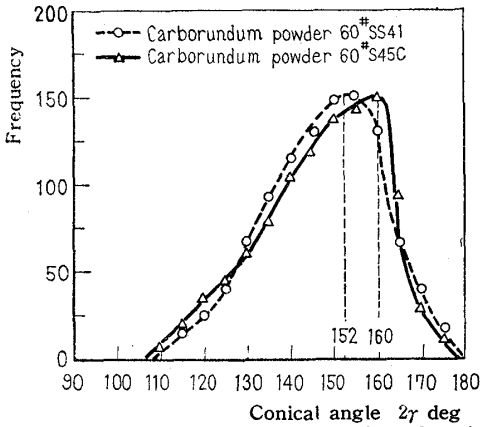


Fig. 10 Distribution of conical angle of surface irregularities

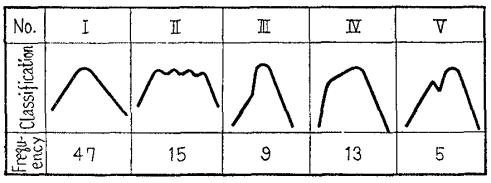


Fig. 11 Profiles of surface irregularities

the number of samples is nearly 1 000.

The values of $k$ in Eq. (19) are listed in Table 6.

(2) $s$-values

Figure 11 shows five main types of profiles of surface irregularities, and they are reduced to the type I after detailed examination.

As a method to transform the various surface irregularities into those profiles of truncated cones, we enlarged by photograpy the profiles of the irregularities as shown in Fig. 12 and the profiles were drawn to the same scale in both ordinate and abscissa.

After that we obtained dimension $d_o$ by the method shown in Fig. 13 and then calculated the $s$-values.

The distribution is shown in Fig. 14. From the figure we see that the specimens have nearly 10 to 20 for $s$-values.

(3) Amount of air-leakage

As above mentioned, amount of air-leakage $Q_i$ is given by Eq. (25), the experimental results of which are shown in Figs. 15 and 16.

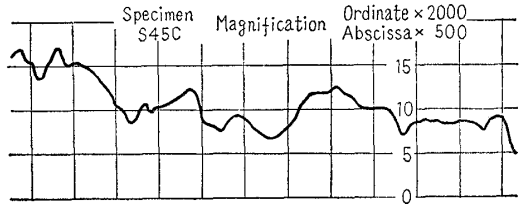


Fig. 12 Enlarged profile of surface irregularities

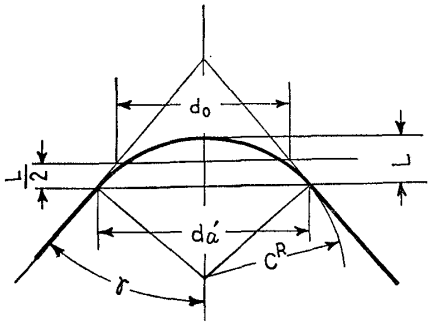


Fig. 13 Calculation method of dimension $d_0$

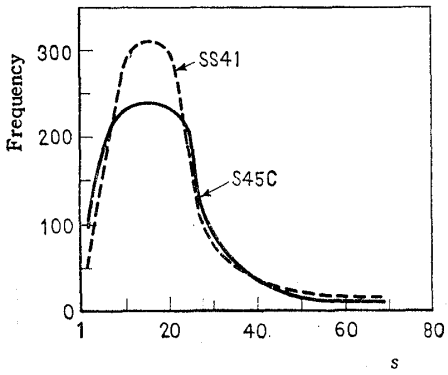


Fig. 14 Distribution of $s$-values

## 6. Considerations

(1) $\gamma$-values The values are regarded as the functions of materials and the processing conditions and others, and have a fairly dispersed distribution as shown in Fig. 10. This phenomenon seems to be caused by using of rough lapping so that an $\gamma$-values may be obtained by using the more raised lapping grade.

(2) $s$-values In the measurement of surface roughness we used Talysurf. As is well known this does not give a true profile of surface roughness because of the roundness at the tip of the palpating needle. However, as is seen from Fig. 12, the minimum size of roundness of the irregularities actually recorded was in the order of 5 microns, so that error in the calculations of $s$-values is supposed to be small.

(3) The values of equivalent gap As shown in Figs. 15 and 16, the air-leakage flow rate at a low initial applied load and that at a low applied load equal to the initial load after applying a maximum applied load show a fairly large difference in spite of identical applied load.

From these results it is inferred that the surface irregularities may be considered practically plastic deformation.

$H_{ep}$-values calculated from these experimental results by means of Eq. (25) are shown in Figs. 17 and 18. From these figures we see that the gap between contact surfaces is practically unchanged in the experimental range; maximum inlet air pressure was below about 1 kg/cm² g. But the deformation

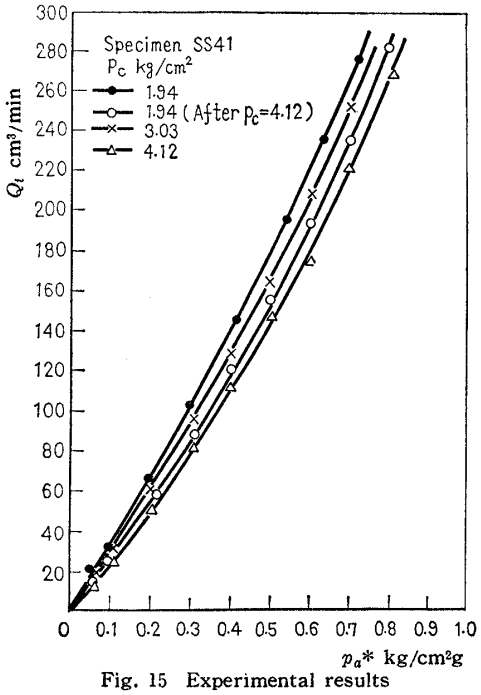


Fig. 15 Experimental results

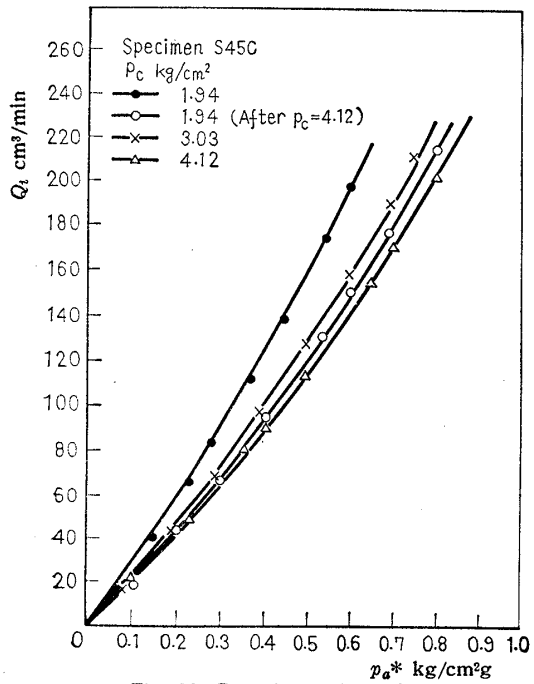


Fig. 16 Experimental results

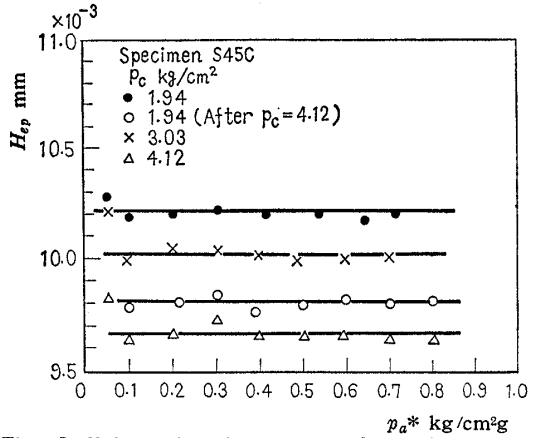


Fig. 17 Values of equivalent gap of experimental results

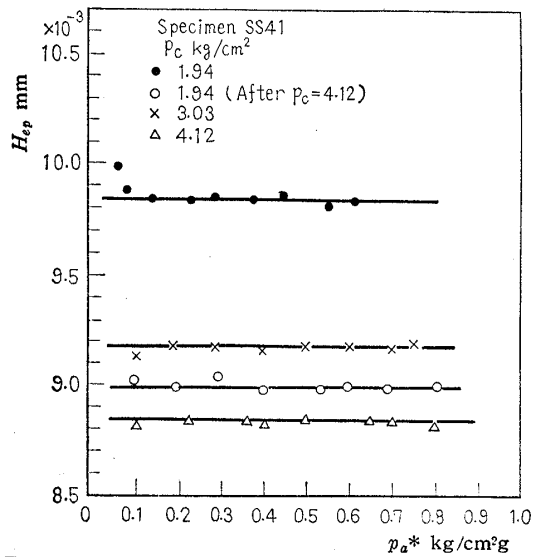


Fig. 18 Values of equivalent gap of experimental results

is not always plastic.

Here, in consideration of the spring back of the surface irregularities, we define as follows:

$$\kappa=\frac{\left[\begin{matrix}\text{Equivalent gap at}\\ \text{initial load after}\\ \text{maximum load}\end{matrix}\right]-\left[\begin{matrix}\text{Equivalent gap at}\\ \text{maximum load}\end{matrix}\right]}{\left[\begin{matrix}\text{Equivalent gap at}\\ \text{initial load}\end{matrix}\right]-\left[\begin{matrix}\text{Equivalent gap at}\\ \text{maximum load}\end{matrix}\right]}\% \quad \cdots\cdots\cdots(26)$$

The elastic behavior rate $\kappa$ for the materials SS 41 and S 45 C, respectively, may be calculated from experimental values as follows.

SS 41: $\kappa=(9.82-9.68)/(10.22-9.68)\fallingdotseq 26\,\%$

S 45 C: $\kappa=(8.98-8.84)/(9.86-8.84)\fallingdotseq 13.7\,\%$

Hence, the values of $\kappa$ for SS 41 is about twice that for S 45 C.

Next, Reynolds number for leakage flow between contact surfaces is given as follows:

$R_e=u(H_{ep})/\nu$

where

$\nu$: kinematic coefficient of viscosity of air

$u$: mean flow velocity of leaking air;

$u=Q/2\pi r(H_{ep})$

From above expression, the maximum value of $R_e$ is obtained as approximately 6, so that the state of leakage flow may be regarded as laminar. The theoretical values of equivalent gap calculated by Eqs. (18) and (23) are listed in Table 7.

Table 7 Equivalent gap (theoretical values)

| $p_c$ kg/cm² | $H_{ep}\times10^{-3}$ mm | | | |
|---|---|---|---|---|
| | SS 41 | | S 45 C | |
| | Plastic deformation | Elastic deformation | Plastic deformation | Elastic deformation |
| 1.94 | 9.96 | 17.92 | 10.29 | 17.61 |
| 3.03 | 9.43 | 17.49 | 9.79 | 17.19 |
| 4.12 | 9.06 | 17.19 | 9.44 | 16.89 |
| $s$ | 15 | | | |

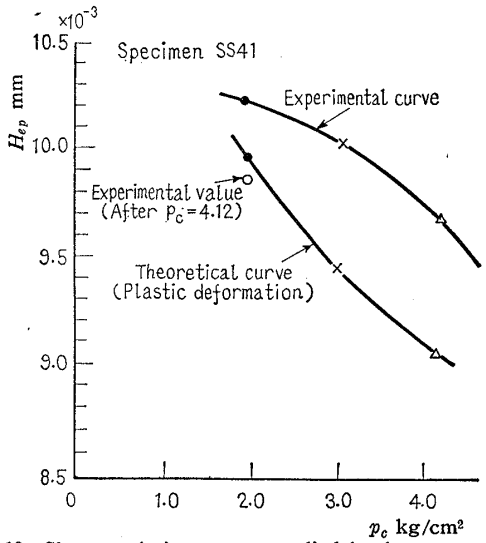


Fig. 19 Characteristic curves; applied load versus equivalent gap

According to above considerations, the deformation of surface irregularities is not elastic, so that the $H_{ep}$-values calculated by Eq. (18) do not apply to either of the materials SS 41 and S 45 C.

Figures 19 and 20 show a comparison between the theoretical values of equivalent gap for plastic deformation listed in Table 7 and the $H_{ep}$-values calculated from experimental results.

As a result of distribution characteristics of $s$-values and $\gamma$-values, theoretical and experimental values of equivalent gap are not necessarily in agreement. Especially in S 45 C, the theoretical values become larger than the experimental values. However, it may be explained as follows. From Figs. 9 and 12 we see that actual surface irregularities do not have their respective cone bases in the supposed base plane. For this reason, the number of surface irregularities actually pressed by applied load becomes smaller than the theoretical value, so that the amount of plastic deformation becomes also larger than its theoretical value and the equivalent gap becomes smaller. Theoretical and experimental values of the rate of decrease of equivalent gap are nearly similar.

The reason why the tendency of the rate of decrease is reversed in the case of SS 41 is not clear.

The deviation of the theoretical values from the

Table 8 Deviations between theoretical and experimental values

| $p_c$ kg/cm² | Deviations % | |
|---|---|---|
| | SS 41 | S 45 C |
| 1.94 | 2.5 | 4.7 |
| 3.03 | 6.0 | 7.0 |
| 4.12 | 6.4 | 6.9 |

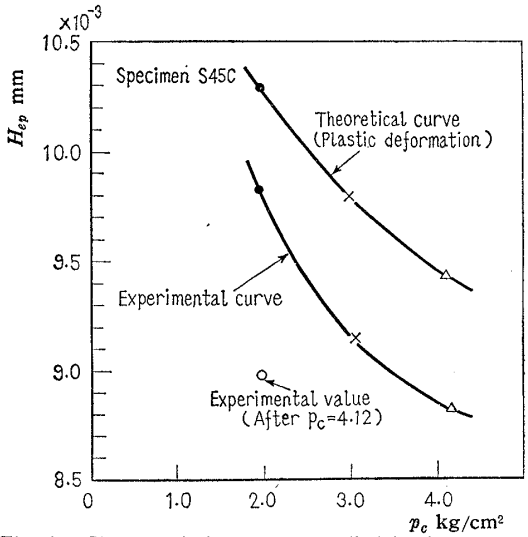


Fig. 20 Characteristic curves; applied load versus equivalent gap

experimental values is listed in Table 8, in which the maximum deviation is about 7 %.

## 7. Conclusions

The phenomenon of fluid leakage between contact surfaces may be considered to be influenced by the following factors:

1) Microgeometric form of the surface irregularities.

2) Elastic and plastic properties of the surface irregularities.

3) Applied load.

4) Fluid pressure.

In this paper, the theoretical expressions with consideration on factors 1), 2) and 3) are obtained, and the results of comparison with experiments are as follows.

(1) In the case in which the specimen was pressed against a rigid smooth surface, assuming its surface irregularities had a form of similar truncated cone, the theoretical values of equivalent gap for the fluid leakage between them were derived as a function of the above three factors. The values obtained by assuming the surface irregularities as ideally plastic were in agreement with the experimental values with deviation within about 7 %.

(2) The deformations of the surface irregularities are fairly plastic. The values of elastic behavior rate $\kappa$ for SS 41 was about twice that for S 45 C.

## Acknowledgement

The author wishes to express his hearty gratitude to Prof. T. Maki, Prof. Y. Furuya, Prof. M. Murakami, Nagoya University and to Prof. Y. Yamada, Nagoya Institute of Technology for their helpful advices. The present study was subsidized by the 1966 Scientific Research Fund, Ministry of Education.

## References

(1) T. Tsukizoe: *Trans. Japan. Soc. Mech. Engrs.*, Vol. 32, No. 239 (1966), p. 1083.
(2) T. Tsukizoe and T. Hisakado: *Trans. ASME*, Ser. D, Vol. 87, No. 3 (1965), p. 666.
(3) V. S. Krasavin: *Report of the Mach. Design Inst., AN SSSR* (1938).
(4) V. N. Marochkin: *Friction & Wear in Machines*, Vol. 13, *Izd., AN SSSR* (1959), p. 79.

## Discussion

**S. Iwanami:** (1) I would like to ask the author about the relation between roughness $H$ and distribution function $f_{(H)}$, the location of the line $H=0$ drawn in Fig. 1, and the relation between the line $H=0$ and the base plane.

(2) I would like to know why the values of $\beta$ are limited in the range of $0.1 \sim 2.0$, as shown in Tables 1 and 2.

(3) I would like to ask about the fastening mechanism between specimen and base plate. If they are clamped by bolts, how much is the elongation of the bolts when fluid pressure is applied?

If the load is induced by the spring force, and a separation between contact surfaces takes place by the contraction of the spring, my question is modified as follows: the contraction of the spring results in a separation between contact surfaces, or does not.

(4) If the experiments in which leakage flow vanished by somewhat large clamping force were performed, I would like to know about the magnitude of the clamping force, the elongation of bolts, and the degree of elastic recovery of the test surface.

**Editorial Director:** (5) As an applied load per unit area is about 2 to 4 kg/cm$^2$, if fluid pressure is around 0.8 kg/cm$^2$g, the actual applied load on the contact surfaces must be less by around 20 %.

The variation of equivalent gap for this change of the applied load is, as shown in Figs. 19 and 20, of the order of 0.2 microns at most, even if it is considered to be elastic deformation, and it is concluded pertinently that no variation appears on a dial gauge.

Accordingly, it is controversial to conclude that the applied load is constant because of no variation of measured value in the dial gauge. I would like to ask whether or not it is supposed that pressure change on the contact surfaces due to variation of inlet air pressure does not influence the equivalent gap because of the plastic deformation of the surface irregularities.

(6) I would like to ask about the comparison with the theoretical results reported in References (1).

**T. Konishi:** (7) I would like to know how to determine $d_o$ from Fig. 13.

(8) The author stated that the deformation of the tip end of surface irregularities was plastic. What were the states of surface irregularities of specimens and of base plate after removal of the applied load? And how did the values of $\gamma$, $s$ and $k$ change as a result? Further, I would like to ask about the relation between the theoretical values of $H_{ep}$ calculated by using these supposedly variable values and the values of $H_{ep}$ obtained from the experiments.

**H. ISHIWATA:** (9) I would like to ask the author about the following matter. It is considered that the theoretical values shown in Figs. 19 and 20 vary according to the values of $h_c$ because of the characteristics of Eqs. (18) and (23). Therefore, I think that the determination of the values of $h_c$ is of large importance.

Consequently, I think that the values of $h_c$ should be determined from the profiles of the surface roughness after the deformation.

(10) The number of surface irregularities actually subjected to deformation by the applied load is supposed to vary with the condition of waviness of surface.

What is the magnitude of waviness? How did you consider the effect of anisotropy of surface roughness?

## Author's closure

(1) The relation between distribution function $f_{(H)}$ and roughness $H$ may be represented graphically as in Append.-Fig. 1.

The principal points in the determination of the values of surface roughness for fluid leakage between contact surfaces may be as follows.

(i) Reference length and its location
(ii) Base plane for roughness $H$
(a) $H=H_{max}$: on the side of contact surfaces
(b) $H=0$: on the base side of truncated cones
(iii) Calculation of the values of $\gamma$, $k$, and $s$

Fundamentally it may be necessary to measure at least more than three places over the whole nominal contact surface as shown in Append.-Fig. 2 (a). In the experiments, the method as shown in Append.-Fig. 2 (b) was used; that is, radial directions; $a$, $b$, $c$=about 5 to 6 mm and tangential directions; $l$, $m$, $n$=about 7 to 8 mm.

In Append.-Fig. 2 (b), the circle shown by a dotted line illustrates the location of the guide metal of the palpating needle.

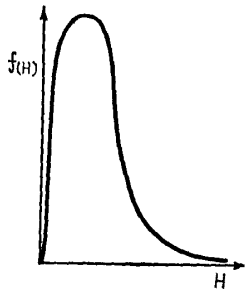


Append.-Fig. 1

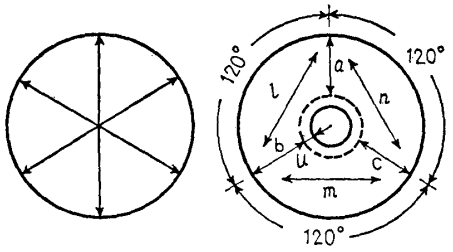


(a) (b)

Append.-Fig. 2

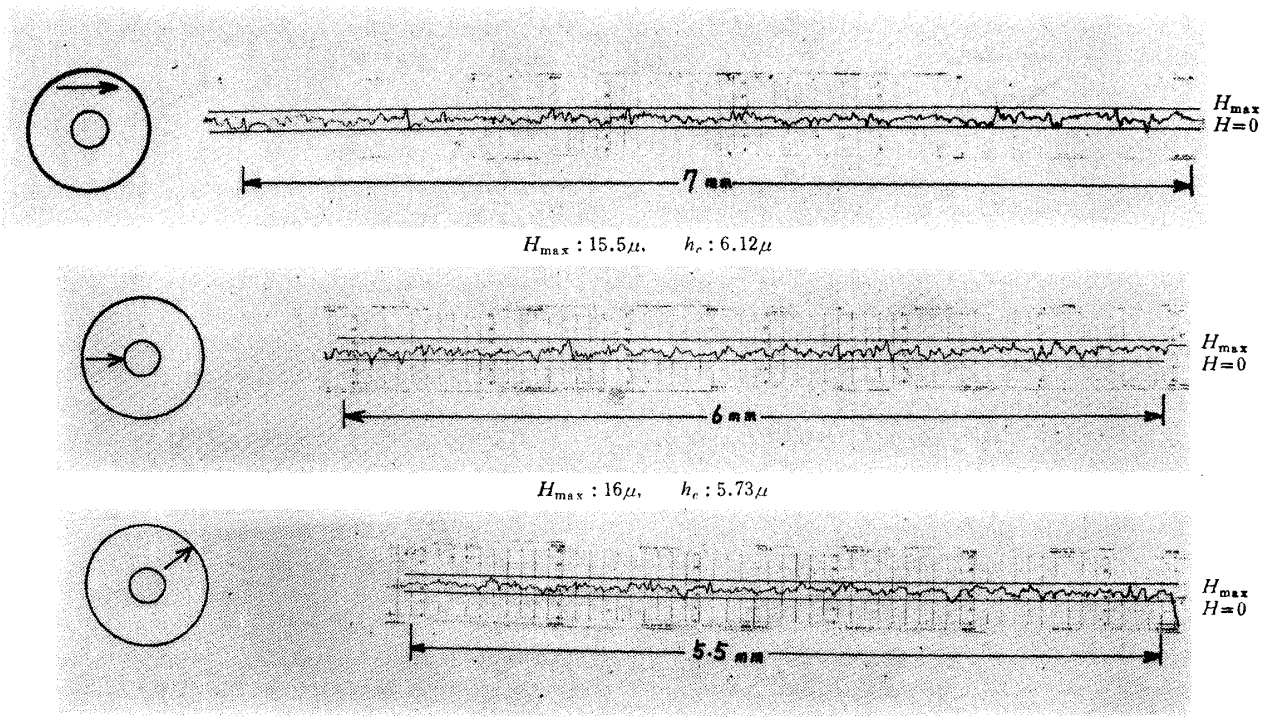


$H_{max}$ : 15.5$\mu$, $h_c$ : 6.12$\mu$

$H_{max}$ : 16$\mu$, $h_c$ : 5.73$\mu$

$H_{max}$ : 13$\mu$, $h_c$ : 5.51$\mu$
Mean value $h_c$: 5.79$\mu$, Specimen: S45C

Append.-Fig. 3 Profiles of surface roughness of specimens

In the range within this circle, the irregularities of the surface can not be surveyed. To the profiles of surface irregularities recorded by the above described method, we draw a plane contacting them at least at three points and denote it by $H=H_{max}$.

Next, let the plane $H=0$ be the plane parallel to this $H_{max}$-plane and cross the deepest part through at least three points.

For the values obtained in six directions by the above method, the numerical values in Table 5 are given as follows; maximum value for $H_{max}$, and mean value for $h_c$. An example is given as Append.-Fig. 3.

(2) Determination of the limit of $\beta$.

The following expression may be derived from the definition of $\beta$.

$$0\leqq\beta\leqq Z_0/\alpha\leqq H_{max}/\alpha \quad \cdots\cdots(i)$$

Using the $\alpha$-value of Eq. (16) in Eq. (i), we have

$$0\leqq\beta\leqq H_{max}/(9\sqrt{\pi}\,\zeta h_c/8)\cong H_{max}/2\zeta h_c \quad \cdots\cdots(i)'$$

Here, if we use the relation $1\leqq s\leqq\infty$ in Eq. (17), we have

$$1/3\leqq\zeta\leqq 1 \quad \cdots\cdots(ii)$$

Now

$$\left.\begin{aligned} h_c/H_{max}&=(1/3)\sim(35/40)^{(a)}\\ &=(1/3)\sim(1/2)\sim(2/3)^{(b)}\\ &\text{(Turning, Grinding, and Buffing, respectively)}\end{aligned}\right\}\cdots\cdots(iii)$$

So using Eqs. (ii) and (iii) on the right side of Eq. (i)', we have

$$H_{max}/2\zeta h_c=\frac{1}{2}\left\{\frac{1}{(1/3)\sim 1}\right\}\left(3\sim\frac{40}{35}\right)$$

$$=4.5\sim 1.7 \text{ for } s=1$$

$$=1.5\sim 0.6 \text{ for } s=\infty$$

However, $s=1$ is impossible. In the case of the base plate used in the experiments, the measurement gave $s=1.5$ as minimum.

So, if we use $s=1.5$, we have $\zeta\fallingdotseq 1/2.48$, so that, using this value in Eq. (i)' and taking into consideration the values of Eq. (iii), we have

$$H_{max}/2\zeta h_c=(1/2)\cdot(2.48)\cdot(3/2\sim 40/35)$$

$$=1.86\sim 1.4$$

Hence, we defined the limit of $\beta$ as $0\leqq\beta\leqq 2.0$

(3)～(4) As the fastening mechanism for specimens and base plate is as shown in Append.-Fig. 4, there is no influence of the clamping bolts on the contact surfaces.

Here, we kept observing the motion of the pin of 3 mm$\phi$ placed on the upper end of push-fittings, Part number *7* in Append.-Fig. 4.

During the experiments a variation of the motion of the pin could not be recognized. The motion was measured by a dial gauge.

Strictly speaking, the contraction of specimens, O-ring fittings, and push-fittings should be taken in to consideration. But, since the spring and these parts are connected in series, no variation of the motion of the pin results in rather little variation of the applied load.

(5) In the range of experiments, the equivalent gap is almost constant as shown in Figs. 17 and 18. But, as a force to separate specimens from the contact surfaces is generated by fluid pressure in the empty space between contact surfaces, the applied load has to be varied as the result. The variations of the applied load are so small that they do not

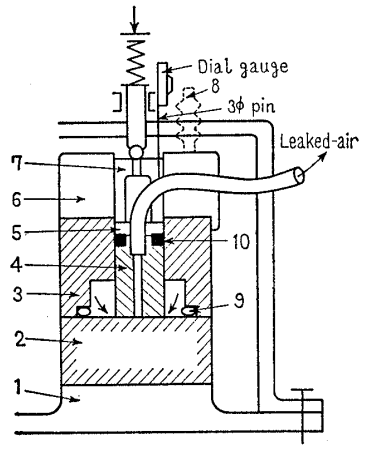


*1*: Bed plate
*2*: Base plate
*3*: Air chamber
*4*: Specimen
*5*: O-ring fittings
*6*: Fittings for air-chamber
*7*: Fittings
*8*: Set-screws
*9* and *10*: O-ring

Append.-Fig. 4

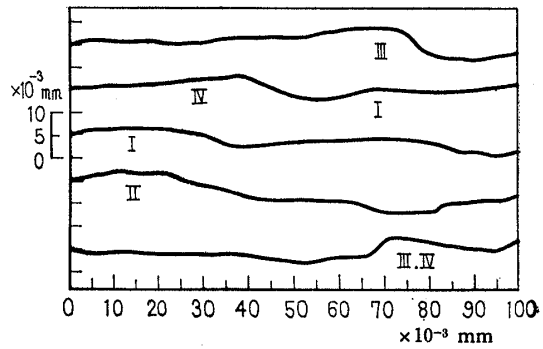


(a) SS41

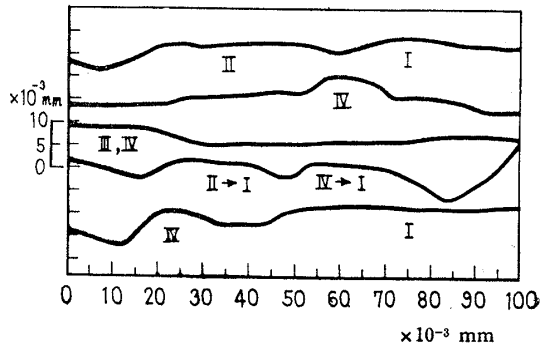


(b) S45C

Append.-Fig. 5 Profiles of surface roughness

(a) Y. Tanaka and T. Saitō: Precision Working, (1962), p. 98, Yokendō.

(b) P. E. D'yachenko, N. N. Tolkacheva, G. A. Andreev, and T. M. Karpova: The Actual Contact Area between Touching Surfaces, (1964), p. 47, Consultants Bureau.

appear in the dial gauge.

But, as you pointed out, the reduction of the applied load is considered not to influence the equivalent gap because the surface irregularities are plastic.

(6) The theoretical results in References (1) were obtained by assuming that the value of flow pressure $p_m$ concerned in contact phenomena between metal surfaces might be constant during plastic deformation of the metal at the contact under an applied load.

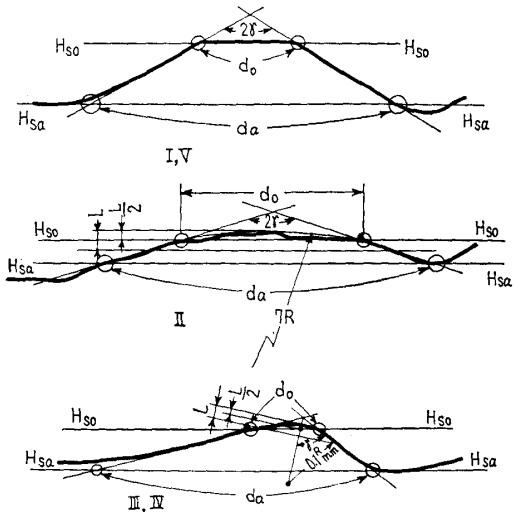


Append.-Fig. 6 Calculation methods for $d_0$ and $d_a$

In this paper, the theoretical values of equivalent gap were derived by assuming that the surface irregularities had a form of similar truncated cone. Accordingly, it seems to be difficult to make an exact comparison of their contents.

However, if compared, the following conclusions may be obtained.

According to Reference (1);

$\delta$ (average clearance) $\propto H$ (maximum height of asperities) in this paper;

$H_{ep}$ (equivalent gap) $\propto h_c$ (central height of surface irregularities)

(7) From the profiles of the surface irregularities enlarged to the same scale for ordinate and abscissa as shown in Append.-Fig. 5, we determined the values of $d_a$ and $d_0$ by using the methods as shown in Append.-Fig. 6, and calculated the $s$-values.

Now, the line $H=0$ given in Append.-Fig. 6 is the one described in the closure to Discussion (1).

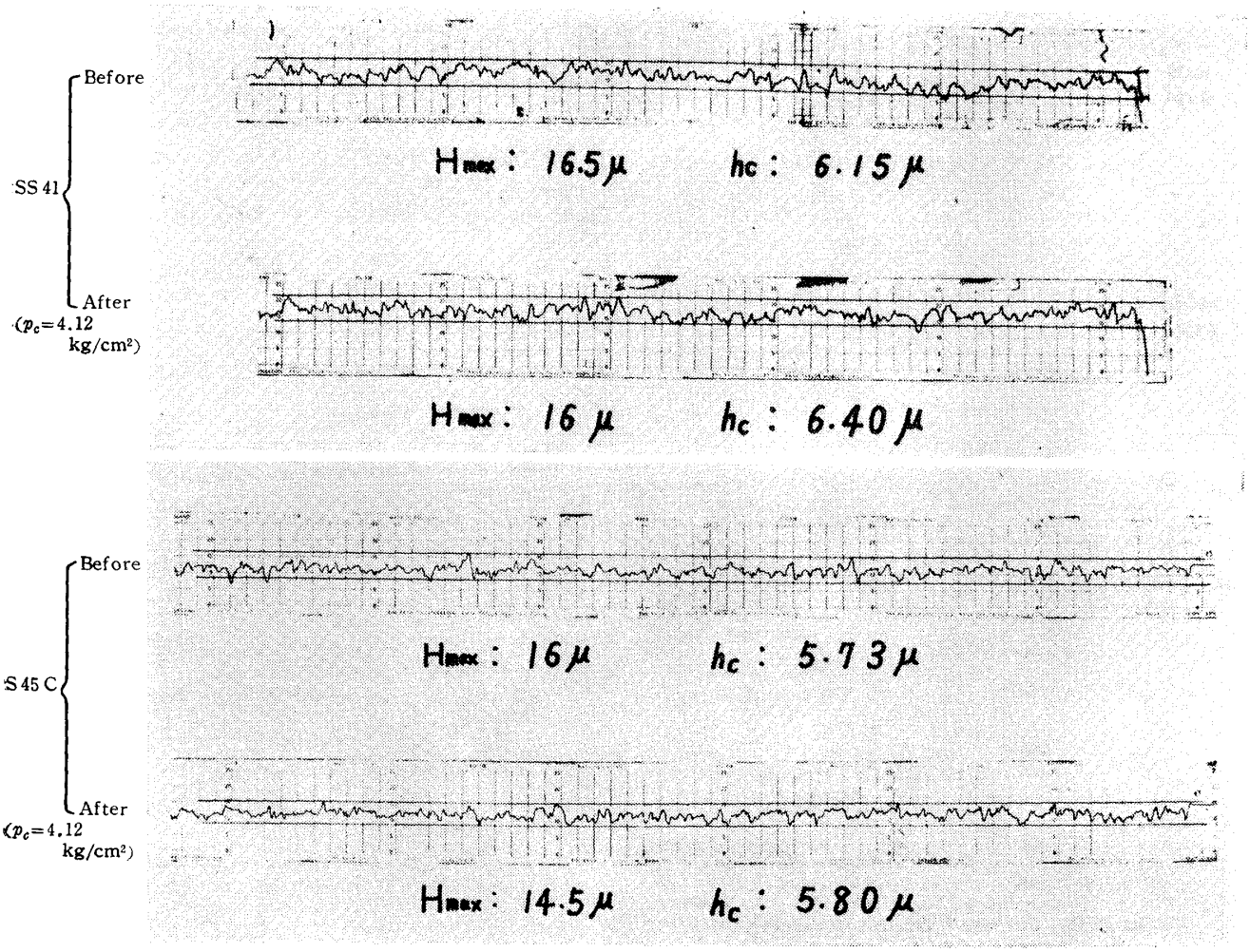


Append.-Fig. 7 Comparison of profiles of surface roughness

(8) As far as the measurements using Talysurf and interference microscope are concerned, there is no confirmation of the change in surface roughness of the base plate before and after the experiments.

As for specimens we think as follows. The profiles of the surface irregularities before and after experiments for supposedly identical places are shown in Append.-Fig. 7.

However, it is difficult to record completely identical places.

Moreover, as is well known, steel has no reproducibility of the profiles of surface irregularities. And the fraction of elastic deformation of the surface irregularities is also included.

Therefore, we cannot draw a strict conclusion, but as a result of statistical investigation of the profiles of the surface irregularities, there was practically no change in the distribution of $\gamma$.

For this reason, we may conclude that $k$-value is also unchanged.

Next, the distribution of $s$ tends to swell slightly toward smaller value but no apparent difference was observed.

The reason may be stated as follows. As is shown in Append.-Fig. 7, since the surface roughness is fairly large, the actual contact area is considered to be small.

Furthermore, the small applied load used in the experiments also results in a small actual contact area.

However, the values of $\gamma$ and $s$ are theoretically considered to be a function of materials (including the condition of heat treatment), applied load, surface roughness, etc., and a study on these points will be continued in future.

Radii $7R$(II) and $0.1R$(III, IV) given in Append.-Fig. 6 are the sizes of the examples.

(9) We think you are right so far as the deformation is concerned which takes place only in the contacting parts without any change in other parts and in which moreover the surface irregularities are ideally plastic. In supplement to the above, we should like to add that the $h_c$-values under the condition of an applied load acting should be used.

By the reason described in the closure to Discussion (8), it is difficult to discover the changed state of surface roughness, but as a result of measurement we could not confirm any difference in $h_c$-values before and after the applied load.

For this reason, we used the $h_c$-values before the load application.

(10) Magnitudes of the waviness of surface are given in Table 5. The actual size of specimens is smaller than the standard length prescribed by JIS, i.e.; the length more than $3\,\text{mm} \times 5 = 15\,\text{mm}$, so that the length described in the closure to Discussion (1) was used. And we used the maximum values for $H_{\max}$ and the mean values for $h_c$. Further, in this paper, it was assumed that the surface roughness were isotropic.